Generalization of the duration-time concept for interpreting high-resolution resonant photoemission spectra

R. Feifel,[1,*] A. Baev,[2] F. Gel'mukhanov,[2,6] H. Ågren,[2] M. N. Piancastelli,[1,7] M. Andersson,[1,†] G. Öhrwall,[1] C. Miron,[1,3,8,†] M. Meyer,[3] S. L. Sorensen,[4] A. Naves de Brito,[5,‡] O. Björneholm,[1] L. Karlsson,[1] and S. Svensson[1]

[1]*Department of Physics, Uppsala University, Box 530, S-751 21 Uppsala, Sweden*

[2]*Theoretical Chemistry, Roslagstullsbacken 15, Royal Institute of Technology, S-106 91 Stockholm, Sweden*

[3]*LURE, Centre Université Paris-Sud, Bâtiment 209D, Boîte Postale 34, F-91898 Orsay Cedex, France*

[4]*Department of Synchrotron Radiation Research, Institute of Physics, University of Lund, Box 118, S-221 00 Lund, Sweden*

[5]*Labóratorio Nacional de Luz Síncrotron (LNLS), Box 6192 CEP: 13084-971 Campinas, Brazil*

[6]*Institute of Automation and Electrometry, 630090 Novosibirsk, Russia*

[7]*Department of Chemical Sciences and Technologies, University "Tor Vergata," I-00133 Rome, Italy*

[8]*Laboratoire Francis Perrin, CNRS-URA 2453-DSM/DRECAM/SPAM CEA Saclay, Bâtiment 522, F-91191 Gif sur Yvette Cedex, France*

(Received 5 September 2003; published 18 February 2004)

The duration-time concept, vastly successful for interpreting the frequency dependence of resonant radiative and nonradiative x-ray scattering spectra, is tested for fine-scale features that can be obtained with state of the art high-resolution spectroscopy. For that purpose resonant photoelectron (RPE) spectra of the first three outermost singly ionized valence states $X\,^2\Sigma_g^+$, $A\,^2\Pi_u$, and $B\,^2\Sigma_u^+$, are measured for selective excitations to different vibrational levels (up to $n=13$) of the N $1s\rightarrow\pi^*$ photoabsorption resonance in N_2 and for negative photon frequency detuning relative to the adiabatic 0-0 transition of this resonance. It is found that different parts of the RPE spectrum converge to the spectral profile of direct photoionization (fast scattering) for different detunings, and that the RPE profiles are asymmetrical as a function of frequency detuning. The observed asymmetry contradicts the picture based on the simplified notation of a common scattering duration time, but is shown to agree with the here elaborated concept of partial and mean duration times. Results of the measurements and the simulations show that the duration time of the scattering process varies for different final electronic and different final vibrational states. This owes to two physical reasons: one is the competition between the fast ''vertical'' and the slow ''resonant'' scattering channels and the other is the slowing down of the scattering process near the zeros of the real part of the scattering amplitude.

DOI: 10.1103/PhysRevA.69.022707 PACS number(s): 33.80.Eh, 33.70.Ca, 34.50.Gb

I. INTRODUCTION

During the last decade our knowledge of resonant Raman x-ray scattering (RXS) has increased considerably, both for the radiative and nonradiative cases which are essentially coherent processes going through a manifold of interfering vibrational levels in the intermediate, core-excited, electronic states [1–5]. The crucial role of lifetime vibrational interference (LVI) [6] on the formation of the RXS spectral profiles is now firmly established. An interesting dynamical aspect of LVI is that the duration of the scattering process is strongly influenced by LVI [4,6–11]. An important question related to this behavior is the dependence of the RXS duration time on the detuning of the photon energy from the photoabsorption resonance. The notation of scattering duration for photon frequency detuning is well established as shown by a number of examples concerning different physical subprocesses [12–20]. There is, however, lack of experimental application of this concept in the region of considerable photoabsorption (see Ref. [4]). According to the simplified picture [12], the scattering duration is sensitive only to the potential-energy surface of the core-excited state, while the experimental spectra presented here demonstrate that an evolution of the spectral profile with change of the detuning frequency is as well very sensitive to the final electronic state and to the final vibrational state. This indicates that a more detailed dynamical characteristic is needed, namely, one in which a partial duration time of the scattering process for each final state is taken into consideration. The aim of the present article is to present an experimental and theoretical investigation of the dynamics involved in the formation of resonant x-ray photoelectron (RPE) spectra at high resolution where these considerations about final-state dependent duration times can be evaluated and experimentally tested.

The paper is organized as follows: The experimental conditions are briefly described in Sec. II, the scheme of computations is outlined in Sec. III, and the experimental spectra together with the numerical simulations are presented and discussed in Sec. IV. The nuclear dynamics, essential for the formation of the RPE profiles, which is related to the ''resonant'' and ''vertical'' scattering channels, is investigated in detail, and an asymmetry of the scattering duration as a function of frequency detuning is studied in Sec. V A. We ana-

*Present address: Physical and Theoretical Chemistry Laboratory, Oxford University, South Parks Road, Oxford OX1 3QZ, United Kingdom.

†MAX-LAB, University of Lund, Box 118, S-221 00 Lund, Sweden.

‡On leave from Department of Physics, University of Brasília, 70910-900 Brasília, Brazil.

lyze the formation of the RPE spectra by making use of the notation of a partial and mean duration time in Sec. V B. The role of the zeros of the scattering amplitude on the spectral profile and on the partial duration time is discussed as well in this section. A short discussion of the duration time concept with respect to the Heisenberg uncertainty principle is given in Sec. V C. Finally our findings are summarized in the last section, Sec. VI.

II. EXPERIMENT

The experimental spectra were recorded at the undulator beamline I 411 [21] at the MAX II storage ring at MAX-lab, Lund, Sweden. This beamline is equipped with a modified Zeiss SX700 plane-grating monochromator covering the energy range 50–1200 eV, and with a rotatable SES 200 high-resolution electron spectrometer using a hemispherical analyzer. For the resonant Auger electron spectra the monochromator bandpass was set to $2\gamma=85$ meV, the spectrometer resolution to 75 meV and the Doppler broadening is estimated to be 50 meV, giving a total resolution of about 124 meV. For the off-resonance spectra ($\hbar\omega=95$ eV) the monochromator contribution was 10 meV, the spectrometer contribution was 30 meV and the Doppler broadening is estimated to be 20 meV, giving a total resolution of about 38 meV. The main axis of the spectrometer lens was set to the ''magic angle'' (54.7°) with respect to the electric-field vector of the linearly polarized synchrotron light. N_2 gas with a stated purity of $>99.99\%$ was commercially obtained. The purity of the gas has been carefully checked by on-line valence photoelectron spectroscopy during measurements. The energy scale of the resonant Auger electron spectra and of the valence-band spectra is calibrated relative to the values given in Ref. [22]. X-ray absorption spectra were recorded around the N $1s\rightarrow\pi^*$ resonance before and after all resonant Auger spectra in order to absolutely calibrate the photon energy.

In some of our experimental spectra we encountered an additional spectral line due to Stokes doubling, which is an instrumental artifact caused by small contribution of non-monochromatic stray light passing through the optical system of the beamline (see Refs. [23,24]). In cases where the Stokes line coincides in binding energy with the resonant Auger lines of interest upon photon frequency detuning, we indicate it in the figure by a dashed line. In cases where the Stokes line was sufficiently far away from the binding energy region of interest, we subtracted it and corresponding spectra are marked by an asterisk. The Stokes doubling for the N_2 molecule is discussed in detail in Ref. [25], where we show that the relative intensity of the Stokes line is strongly related to the detuning of the undulator harmonic. The interested reader may refer to this work for further discussion.

III. NUMERICAL SIMULATIONS

In order to compare the experimental data with theory we performed numerical simulations. In these calculations the RPE cross section is computed as the following [4]:

$$\sigma(E,\omega)=\int \sigma^0(E,\omega')\Phi(\omega'-\omega,\gamma)d\omega',$$

$$\sigma^0(E,\omega)=\sum_m \sigma_m^0(E,\omega),$$

$$\sigma_m^0(E,\omega)=|F_m|^2\Delta(\omega-E-\omega_{00}^{f0}-\varepsilon_m^f,\Gamma_f). \qquad (1)$$

In the simulations we used the binding energy, $\mathrm{BE}=\omega-E$, instead of the kinetic energy of the Auger electron, E. The spectral function of the incident radiation is assumed to be Gaussian, $\Phi(\Omega,\gamma)=[\exp(-\Omega^2/\gamma^2)\ln 2]\sqrt{\ln 2}/\sqrt{\pi}\gamma$, with γ as half width at half maximum (HWHM). The small final-state lifetime broadening is neglected in these numerical simulations ($\Gamma_f=0$).

The Kramers-Heisenberg (KH) amplitude of the RPE process

$$F_m=\sum_n F_{mn},\quad F_{mn}=\frac{\langle m|n\rangle\langle n|0\rangle}{\Omega-\varepsilon_n^c+\imath\Gamma} \qquad (2)$$

written within the Born-Oppenheimer approximation depends on the Franck-Condon (FC) amplitudes between the ground $|0\rangle$, core excited $|n\rangle$, and final $|m\rangle$ vibrational states. The labels 0, c, and f mark the ground, core-excited, and final electronic states, respectively, while 0, n, and m are the vibrational quantum numbers of the electronic states 0, c, and f, respectively. Γ denotes the natural lifetime width of the core-excited state [$\Gamma=0.0575$ eV (HWHM) for N_2], and Ω is the detuning of the photon frequency ω from the nominal resonant frequency. For the present case of N $1s\rightarrow\pi^*$ core excitation in N_2 we define the nominal resonant frequency as the photoabsorption transition $0\rightarrow c$ between the lowest vibrational levels $0\rightarrow 0$ of ground 0 and core-excited c states, ω_{00}^{c0}, and Ω reads as $\Omega=\omega-\omega_{00}^{c0}$. It is worth noting that ω_{00}^{c0} for the N $1s\rightarrow\pi^*$ resonance in N_2 is close to the frequency of the vertical transition as can be seen from the NEXAFS-spectrum (see, e.g., Refs. [26,29]).

We omit in F_{mn} [Eq. (2)] the prefactor which depends on the electronic transition matrix elements. Furthermore we are using atomic units and the notation $\varepsilon_n^c=\epsilon_n^c-\epsilon_0^c$, where $\epsilon_n^c=\omega_c[n+1/2-x_c(n+1/2)^2]$ is the vibrational energy of the core-excited state with the anharmonicity $\omega_c x_c$. In the harmonic approximation, $\varepsilon_n^c\approx n\omega_c$, where ω_i is the vibrational frequency of the ith electronic state.

For the Franck-Condon factor calculations we used Morse potentials based on spectroscopical constants from Huber-Herzberg (cf. Ref. [27]) for the neutral ground and the singly ionized final states. Recently, we extracted from the resonant photoelectron data [28] of the $X\,^2\Sigma_g^+$ final state in N_2 and from NEXAFS data [29], the equilibrium internuclear distance and vibrational frequencies for the N $1s\rightarrow\pi^*$ core-excited state, respectively (see Table I). As it is pointed out in Ref. [29], the resonant Auger decay to the singly ionized final $A\,^2\Pi_u$ state following excitations to high vibrational levels of the core-excited state, seemed to be very sensitive to the anharmonicity of the core-excited state. Therefore we performed a curve-fitting data analysis of our experimental

TABLE I. Spectroscopic constants used for calculations of the Morse potential curves.

	ω_e (cm^{-1})	$\omega_e x_e$ (cm^{-1})	R^0 (Å)	E_{00} (eV)	Refs.
N_2 ($X\,^1\Sigma_g^+$)	2358.57	14.324	1.09768	0	[26]
N*N ($^1\Pi_u$)	1904.1	17.235	1.1645	400.88	[28]
N_2^+ ($X\,^2\Sigma_g^+$)	2207.00	16.10	1.11642	15.581	[26]
N_2^+ ($A\,^2\Pi_u$)	1903.70	15.02	1.1749	16.689	[26]
N_2^+ ($B\,^2\Sigma_u^+$)	2419.84	23.18	1.0742	18.751	[26]

resonant Auger data for the $A^2\Pi_u$ final state in order to extract the spectroscopical constants for the N $1s\rightarrow\pi^*$ core-excited state in an alternative way. However, we did not obtain a significant difference from the spectroscopical constants determined recently by Refs. [28,29]. Thus we used in the simulations the spectroscopical constants from Refs. [28,29], which are summarized in Table I.

IV. RESULTS

Figures 1 and 2 show resonant Auger decay spectra of the first three outermost singly ionized valence states $X\,^2\Sigma_g^+$, $A\,^2\Pi_u$ and $B\,^2\Sigma_u^+$, measured for selected excitations to different vibrational levels of the N $1s\rightarrow\pi^*$ photoabsorption resonance in N_2 and for negative photon frequency detuning relative to the adiabatic 0-0 transition of this resonance, respectively. Corresponding off-resonance spectra recorded at a photon energy of $\hbar\omega=95$ eV are also included for comparison. In Fig. 1, excitations up to the vibrational level $n=13$ were investigated. As recent high-resolution photoabsorption spectra of N_2 show sufficient population of vibrational levels up to only $n=7$ in the N $1s\rightarrow\pi^*$ core-excited state (see Refs. [26,29]), the experimental photon energies corresponding to the vibrational levels $n>7$ of the core-excited state were calculated assuming a Morse potential for the core-excited state, based on the recently obtained spectroscopical constants from Refs. [28,29] (see Table I). A similar experimental procedure was reported earlier for C $1s\rightarrow\pi^*$ core-excited CO (see Ref. [30]). In Fig. 3 we show a detail of the experimental and numerical RPE spectra of N_2 for the singly ionized $A\,^2\Pi_u$ final state, where the excitations were altered between ''on top'' and ''in between two vibrational levels.''

As we can see from Figs. 1– 3, the numerical simulations presented alongside the experimental results show good agreement with the experiment save for the $B\,^2\Sigma_u^+$ final state. Reasons for the deviations encountered in the *B*-final states are manifold according to Ref. [31]. Equation (2) neglects the amplitude of the direct photoionization process which is known to be important for this particular final state (see Ref. [31]). Furthermore, the decay rates for the transition from the core-excited to the final $B\,^2\Sigma_u^+$ state are shown in Ref. [31] to strongly depend on the internuclear bond distance due to configuration interaction with the neighboring $C\,^2\Sigma_u^+$ state in N_2^+. This is not accounted for in the presented simulations. As these peculiarities of the $B\,^2\Sigma_u^+$ state have been discussed in great detail in Ref. [31], we would not elaborate this discussion in the following.

In contrast, for the singly ionized $X\,^2\Sigma_g^+$ and $A\,^2\Pi_u$ final states we can estimate from our experimental data that the direct channel compared to the resonant channel is, on top of the π^* resonance, $<1\%$. Therefore, the neglect of the direct channel in Eq. (2) is justified for the $X\,^2\Sigma_g^+$ and $A\,^2\Pi_u$ final states in very good approximation. This is corroborated by

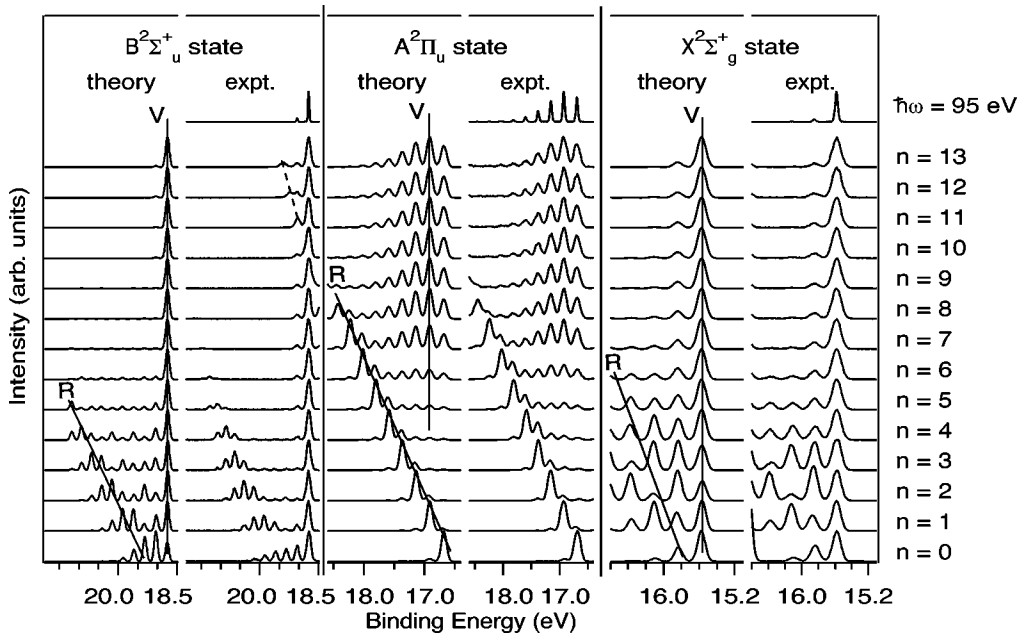

FIG. 1. Experimental and numerical RPE spectra of N_2 for different final states for positive detuning. Resonant excitation to certain core-excited vibrational levels is considered. The highest panels show the spectra of direct photoemission. The ''resonant'' and ''vertical'' bands are marked by labels *R* and *V*, respectively.

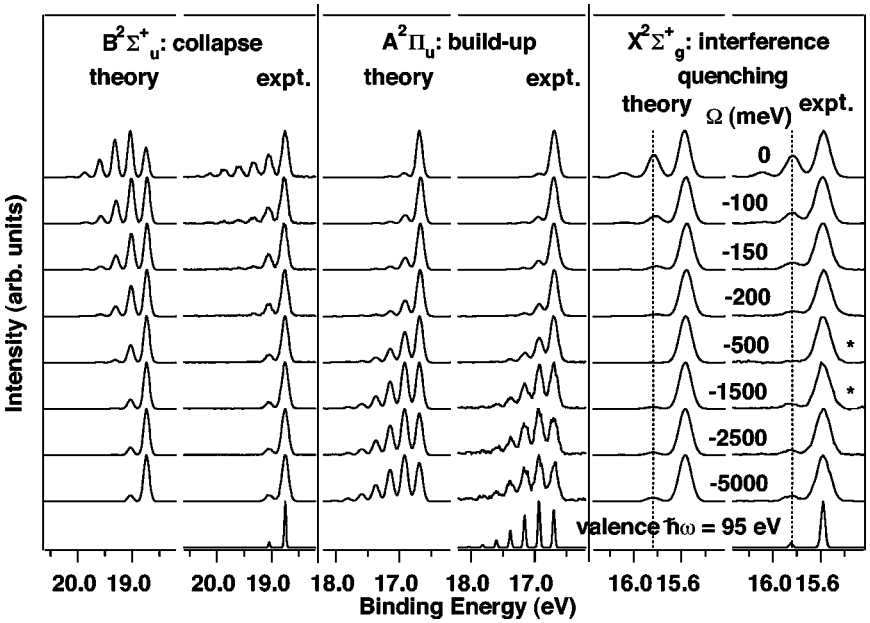

FIG. 2. Experimental and numerical RPE spectra of N_2 for different final states for negative frequency detuning. The lowest panels show the spectra of direct photoemission.

the good agreement between the experiment and the numerical simulations and shows that a resonant consideration is indeed applicable for the $X\,^2\Sigma_g^+$ and $A\,^2\Pi_u$ final states in the following discussion.

By looking closely at Fig. 1, we can see that all three outermost singly ionized valence states of N_2 resemble the intensity distribution of the direct photoionization spectrum for an excitation to $n=13$. Note that the feature marked by a dashed line in the $B\,^2\Sigma_u^+$ final state is due to Stokes doubling of the A state [25] and should not be confused with an excited final-state vibrational line component of the B-final state (see also Sec. V A 1). The question of interest for the following discussion is if all three electronic states converge to the direct photoionization spectrum at the same excitation energy. As we can see, the group of lines on the higher-binding-energy side of the $B\,^2\Sigma_u^+$ final state, which are known from Ref. [31] to be of pure resonant nature, has completely vanished for all excitations $n>7$. Furthermore, the $X\,^2\Sigma_g^+$ final state resembles the vibrational envelope of the direct photoionization for $n>8$, and the A state reaches the intensity distribution of direct photoionization for $n>9$. This shows that different electronic states converge to the direct photoionization limit for different photon energies.

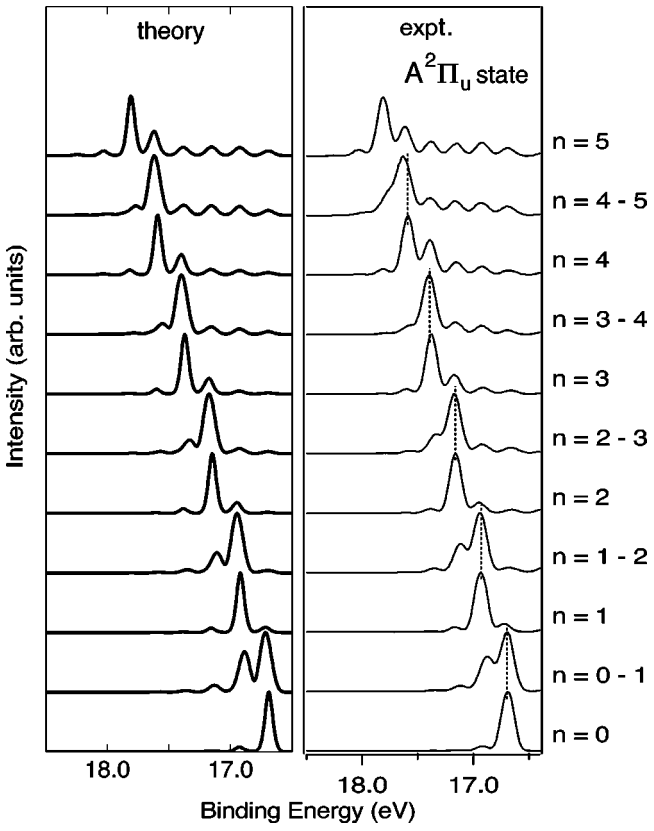

FIG. 3. Experimental and numerical RPE spectra of N_2 for the singly ionized $A\,^2\Pi_u$ final state, alternating the excitation on top and in between two vibrational levels.

In addition to that, the $A\,^2\Pi_u$ final state exhibits an interesting behavior. For excitations up to $n=6$, the strongest final-state vibrational line m corresponds to the excited intermediate state vibrational level n. In particular, for excitation to $n=0$ the final-state vibrational line $m=0$ is dominant, for excitation $n=1$ the final-state vibrational line $m=1$ is dominant etc. This peculiar behavior is even more elaborate in Fig. 3, where we follow the development of the dominant final state vibrational line both for ''on top'' and ''in between'' excitations. Such a behavior of the $A\,^2\Pi_u$ final state has already been reported earlier by Ref. [32], however, the data interpretation was at that time limited due to lower-energy resolution. Returning our attention to the middle panel of Fig. 1, we can see that for excitations $n>6$ the vibrational envelope shows two subgroups of lines, one at the lower-binding-energy side and the other one at the higher-binding-energy side of the $A\,^2\Pi_u$ final state. The groups of lines on the lower-binding-energy side show an intensity distribution which is very reminiscent of the intensity distribution of the direct photoionization, whereas the

higher-binding-energy side is different and can be considered being of pure resonant character, in analogy to the situation encountered in the $B\,^2\Sigma_u^+$ final state (see Ref. [8]). This behavior suggests that different parts of the same electronic state reach the direct photoionization limit for different detuning values Ω.

By looking more closely at Fig. 2, we can see that for negative photon frequency detuning the resonant vibrational progressions of the $X\,^2\Sigma_g^+$ and $B\,^2\Sigma_u^+$ final states have almost completely vanished for comparatively small detuning values ($\Omega \approx -150$ meV), whereas the $A\,^2\Pi_u$ final state builds up a vibrational progression upon negative frequency detuning, converging to the intensity distribution of direct photoionizaton. The behavior seen in the N_2 singly ionized $X\,^2\Sigma_g^+$ and $B\,^2\Sigma_u^+$ final states has earlier been observed for the singly ionized $X\,^2\Sigma^+$ state in CO and was noted as ''the collapse of the vibrational fine structure'' (see Refs. [15,16]). Furthermore, a behavior similar to the N_2 singly ionized $A\,^2\Pi_u$ final-state has been observed for the $B\,^2\Sigma^+$ final state in CO^+ and is referred to as the buildup of the vibrational fine structure in the literature (see Refs. [15,16]). An important condition for the collapse effect to take place is that the ground and final state potential curves have approximately the same equilibrium bond distance, whereas for the buildup effect the core-excited state and final state potential curves have to coincide approximately in equilibrium bond distance. Indeed, as we can see from Table I, the conditions for the collapse effect are well fulfilled for $X\,^2\Sigma_g^+$ and $B\,^2\Sigma_u^+$ final states and the conditions for the buildup effect are well fulfilled for the $A\,^2\Pi_u$ final state.

The identification of the collapse effect for the $B\,^2\Sigma_u^+$ final state is somehow problematic due to the fact that already on top of the π^* resonance direct photoionization is known to be important (see Ref. [8]). However, the almost instantaneous breakdown of the long extended vibrational progression ($\Omega \approx -100$ meV) indicates the presence of the collapse effect for this final-state. Furthermore, as was recently shown in Refs. [28,33], the collapse of the $X\,^2\Sigma_g^+$ is not a monotonic function of frequency detuning, but an interference quenching of the $m=1$ final-state vibrational line occurs. This is seen in the right panel of Fig. 2 and in Fig. 4, where we plot the ratio of integrated intensities of the $m=1$ and $m=0$ final vibrational lines as a function of frequency detuning. As we can see from Figs. 2 and 4, the intensity distribution of direct photoionization of the $X\,^2\Sigma_g^+$ is first reached for a detuning $\Omega \approx -150$ meV before the quenching occurs, and for a detuning $\Omega < -2500$ meV after the relaxation of the quenching. Moreover, the $A\,^2\Pi_u$ final state reaches the direct intensity distribution for $\Omega < -1500$ meV. From these considerations we can conclude that similar to the situation for positive detuning, the spectral profile of different final electronic states converges to the intensity distribution of direct photoionzation differently also for negative detuning.

V. DISCUSSION

As we have seen from Figs. 1 and 2, the RPE spectral shape converges to the same profile for large positive and negative detunings. As it is known from Refs. [4,34], the RPE profile for large $|\Omega|$ coincides with the spectral profile of the direct photoemission (see the highest and lowest panels in Figs. 1 and 2, respectively). This limiting case corresponds to the fast RPE according to the approximate expression for the RPE scattering duration time [4,34]

$$\tau \approx \frac{1}{\sqrt{\Omega^2+\Gamma^2}}. \tag{3}$$

This rough estimation shows that the formation of the profile of the fast RPE is the same for positive and negative detunings. However, both experiment and theory (Figs. 1 and 2) show the opposite trend, namely, the RPE process for the A-final state starts to converge to the profile of the direct photoionization (to be fast) for $\Omega \gtrsim 2$ eV and $\Omega \lesssim -1.5$ eV. The main reason of a such an Ω asymmetry [4] and break down of Eq. (3) is that contrary to negative detunings $\Omega<0$, the photon frequency is in resonance with some vibrational level n if $\Omega>0$. A similar nonsymmetric Ω behavior has also been observed recently in the more complex system of the polyatomic molecule BF_3, where the asymmetric Ω behavior was discussed to reflect the partial RPE cross section from the outer classical turning points rather than in the convergence limit to the fast RPE spectral profile [35]. Finally, we would like to point out another peculiarity: The transition to the fast limit is different for different final states. Let us explore in more details the Ω asymmetry of the formation of the fast RPE spectral profile.

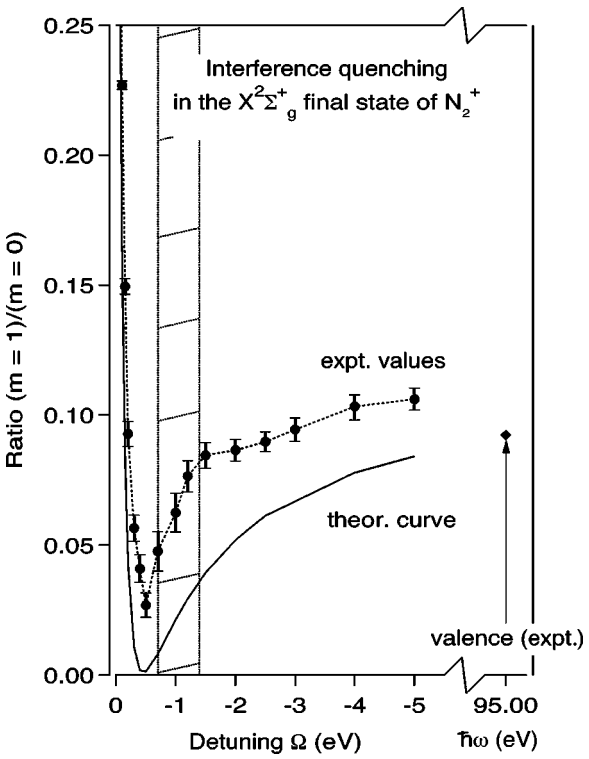

FIG. 4. Ratio $(m=1)/(m=0)$ of the integrated intensities for the singly ionized $X\,^2\Sigma_g^+$ final state of N_2 as a function of detuning Ω.

A. Asymmetry of the scattering as a function of detuning

The simplified formula Eq. (3) says that the RPE duration depends on the natural lifetime of the core-excited state Γ and on the detuning Ω. However, Eq. (3) neglects a dependence of the RPE duration time on the final state. As it was mentioned earlier in Ref. [34] (see also Sec. II) the duration time of the scattering process can be different for different final states. Let us start from a rather simple physical motivation why the duration time is sensitive to the final electron-vibrational state.

An important conclusion can be drawn directly from Eq. (3), namely that the scattering is slow on resonance ($\Omega=0$; long duration time τ) and fast for large detuning, off resonance (short duration time τ). These two qualitatively different cases will be referred to as ''slow'' and ''fast'' scattering processes in what follows. The amplitude of the fast scattering [34]

$$F_m \approx F_m^S \equiv \frac{\langle m|0\rangle}{\Omega-\varepsilon_v+\imath\Gamma}, \quad [\Omega<\Omega_-;\ \ \Omega>\Omega_+] \qquad (4)$$

is proportional to the FC amplitude $\langle m|0\rangle$ of the direct electronic transition of the nuclear subsystem from the ground to the final vibrational states. As was mentioned in the beginning of Sec. V the scattering starts to be fast differently for positive and negative detunings, $\Omega_+ \neq |\Omega_-|$ (see also Sec. III). For example, the corresponding marginal detunings for the A state are $\Omega_+ \approx 2$ eV and $\Omega_- \approx -1.5$ eV. A similar picture can be encountered for the resonant Auger decay of C $1s \rightarrow \pi^*$ core-excited CO to the $X\,^2\Sigma^+$, where one can see from Refs. [16,30] that the intensity distribution of direct photoionization is reached for negative detuning for $\Omega_- \approx -0.45$ eV, whereas for positive frequency detuning at least $\Omega_+ \approx +1.4$ eV is required.

Equation (4) shows that the spectrum of the ''fast'' RPE copies the spectrum of direct photoemission and manifests itself nicely, for example, in the ''collapse of vibrational fine structure in the Auger resonant Raman spectrum'' (see Refs. [15,16]). Here $\varepsilon_v = U_c(R_0) - \varepsilon_0^c$ is the energy of the vertical transition relative to the lowest vibrational level of the core-excited state. For N_2: $\varepsilon_v \approx \mu\omega_c^2(R_0-R_c)^2/2 - \omega_c/2 \approx n_v\omega_c \approx 92$ meV with the vibrational quantum number of the vertical transition $n_v \approx 0$.

1. Positive detuning: Competition between resonant and vertical scattering channels

Let us first consider the scattering process for positive detuning as shown in Fig. 5. To be a little bit more specific, we consider here the potential surfaces $U_0(R)$, $U_c(R)$ and $U_f(R)$ which model qualitatively the RPE process for the $A\,^2\Pi_u$ final state in the N_2 molecule, where $U_c(R)$, and $U_f(R)$ have close potential shapes according to Table I. In this case $\langle m|n\rangle \approx \delta_{n,m}$.

The scattering amplitude has a maximum when the numerator is large or the denominator of F_m [Eq. (2)] is small. The first case corresponds to the vertical photoabsorption transition with the vibrational energy $\varepsilon_v \approx n_v\omega_c$ ($n_v \approx 0$ for N_2). When ω is tuned away from the vertical transition, the denominator of the scattering amplitude F_m, $\Omega - \epsilon_n^c + \imath\Gamma \approx \Omega - \epsilon_v$, becomes large. However, the smallness of $1/(\Omega-\epsilon_v)$ is compensated by the large FC amplitudes $\langle n_v|0\rangle$ of the vertical transition. The scattering amplitude corresponding to this vertical (V) scattering channel can be estimated as follows:

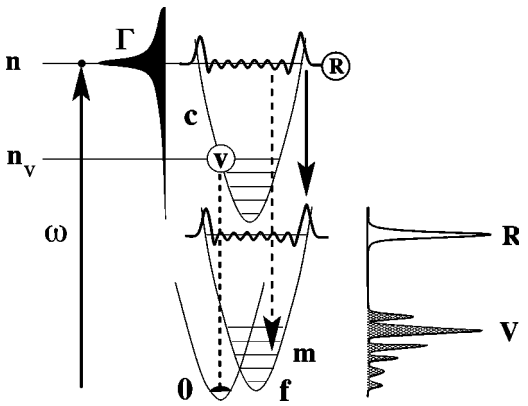

FIG. 5. Formation of vertical and resonant RPE profiles. Labels R and V correspond to resonant, Eq. (6), and vertical, Eq. (5), scattering channels. The shaded profile shows the Lorentzian of core excitation with HWHM$=\Gamma$.

$$F^V \equiv F_{m_v} \approx \frac{1}{\Omega-\varepsilon_v}\sum_{n_v}\langle m_v|n_v\rangle\langle n_v|0\rangle$$
$$\approx \frac{\langle m_v|0\rangle}{\Omega-\varepsilon_v} \sim \frac{1}{\Omega-\varepsilon_v}. \qquad (5)$$

It is not difficult to understand that the RPE band of the vertical channel (marked as V in Fig. 5) follows the Raman dispersion law $E \approx \omega - \omega^{cf}_{n_v,m}$ (the vertical channel is seen as a broad band in the spectrum of the A state, see Fig. 1). Here $\omega^{cf}_{n_v,m} = E_{cn} - E_{fm}$ is the resonant frequency of the decay transition. The comparison of Eqs. (4) and (5) shows that the vertical band converges to the fast limit for large $|\Omega|$.

Let us consider now the second case, when the x-ray photon energy is resonant with some core-excited vibrational state $n \neq n_v$ (cf. Fig. 5). Now the smallness of the FC amplitudes $\langle n|0\rangle$ (which becomes small when ω is tuned away from the vertical transition) is compensated by a small denominator $\sim\Gamma$ in F_m. The corresponding resonant scattering amplitude can be estimated as

$$F^R \equiv F_m \approx \frac{\langle m|n\rangle\langle n|0\rangle}{\Omega-n\omega_c+\imath\Gamma} \approx \delta_{mn}\frac{\langle n|0\rangle}{\Omega-n\omega_c+\imath\Gamma}$$
$$\approx \delta_{mn}\frac{e^{-\eta^2/2}\eta^n/\sqrt{n!}}{\imath\Gamma}, \quad n \approx \frac{\Omega}{\omega_c} > 0. \qquad (6)$$

Here $\eta = (R_c - R_0)/a\sqrt{2}$, $a = 1/\sqrt{\mu\omega_c}$. Contrary to the vertical channel, the resonant channel does not follow the Raman dispersion. For example, the peak position $E \approx \omega^{cf}_{n,n}$ of the narrow resonant band for the A state of N_2^+, Eq. (1), does not depend on the excitation energy $\omega = \omega^{c0}_{n,0}$. Hence it

will stay fixed on the kinetic-energy scale and will disperse on the (presented) binding-energy scale in Figs. 1 and 3, respectively, as a function of frequency detuning. *Caution*: One might easily relate the additional spectral features marked by a dashed line in the spectra of the *B* state (see Fig. 1) to the resonant scattering channel of the *A* state (which is too weak in this region). The origin of these additional spectral features is, however, the non-Raman band of the *A* state caused by Stokes doubling. The broad stray light excitation results in the collapse of the *A* band which one can see as these additional spectral features (for further reading see Ref. [25]).

The comparison of Eqs. (5) and (6) shows that the resonant amplitude F^R decreases faster than F^V with an increase of the detuning. The amplitudes F^R and F^V have the same order of magnitude for vibrational state n_c (or detuning $\Omega = n_c\omega_c$),

$$n_c - n_v \approx \frac{\Gamma}{\omega_c}\frac{\sqrt{n_c!}\,e^{\eta^2/2}}{\eta^{n_c}}. \tag{7}$$

For the N_2 molecule with $\eta \approx 1$ this is expected to occur when $n_c \sim 10$.

The explicit simulations show that it occurs for $n_c \approx 9$ for the $A\,^2\Pi_u$ and for $n_c \approx 6$ for the $B\,^2\Sigma_u^+$ final states, respectively (see Fig. 1). Hence, the off-resonant vertical scattering starts to dominate when

$$\Omega > n_c\omega_c\,. \tag{8}$$

Thus, the RPE spectrum resembles for detunings larger than $n_c\omega_c$ the direct photoemission and the RPE process can be treated as fast. One can see nicely from Fig. 1 that the resonant Auger spectra of N_2 split up into resonant and vertical bands. Both experimental and simulated RPE spectra of the *A*-final state (see Fig. 1) show clearly that with increasing detuning the broad low-binding-energy part of the spectrum (vertical scattering) tends to the spectrum of direct photoemission or fast RPE.

As we can see from Fig. 1, the spectrum changes continuously with increasing ω, when ω is tuned strictly on resonance to the nth vibrational level, $\Omega = \omega_{n0}^{c0}$. However, when the excitation energy is tuned between two vibrational states $n+1$ and n ($\omega = (\omega_{n+1,0}^{c0} + \omega_{n,0}^{c0})/2$), as shown in Fig. 3, the spectrum differs considerably from the resonant spectrum ($\omega = \omega_{n+1,0}^{c0}$ or $\omega = \omega_{n,0}^{c0}$). The reason for this is that in this case both vibrational levels $n+1$ and n are populated and the $(n+1)$th and nth scattering channels compete with each other.

So far, we have demonstrated that for small n_v the scenario of a transition to the spectrum of fast scattering is qualitatively different for negative and positive detunings relative to the frequency of vertical transition, $\Omega - \varepsilon_v$. Indeed when $\Omega - \varepsilon_v$ is negative the resonant region ($0 \leqslant n \leqslant n_v$) is small compared to the case of positive detuning, $\Omega - \varepsilon_v > 0$, where the resonant region is $n_v \leqslant n \leqslant n_c$. Clearly, this asymmetry becomes smaller when the vertical transition corresponds to excitation of high vibrational levels, $n_v \gg 1$ (except excitation near a dissociation threshold). The presented analysis allows us to conclude that the resonant scattering is the slower channel in comparison with the fast vertical channel.

2. Negative detuning

Comparison of Figs. 1 and 2 shows that when $\Omega < 0$ the RPE profile converges faster to the profile of the direct photoemission [Eq. (4)] in comparison with $\Omega > 0$. The main reason for this is that all photoabsorption resonances lie in the region $\Omega > 0$ which is above the bottom of the core-excited potential $U(R)$. According to equation $\tau = 1/[(\omega - \omega_{n0}^{c0})^2 + \Gamma^2]^{1/2}$ the RPE near these resonances is slow, contrary to off-resonant region $\Omega < 0$ where the scattering is faster.

B. Partial and mean durations of the scattering process

1. Partial duration of scattering

To analyze the experimental data further, we need a quantitative definition of the partial duration time τ_m of the scattering process which depends on the final state. The definition of the RPE duration time is not unique [34]. The main reason for this is the absence of a time operator in quantum mechanics. Here we define the RPE duration time as the expectation time

$$T_m = \frac{1}{F_m}\int_0^\infty t\,\mathcal{F}_m(t)\,dt, \tag{9}$$

with the "'density" $\mathcal{F}_m(t)$ and the RPE amplitude of the decay at time *t*,

$$F_m = \int_0^\infty \mathcal{F}_m(t)\,dt,$$

$$\mathcal{F}_m(t) = -\imath e^{-(\Gamma - \imath(\omega + E_0))t}\langle m|e^{-\imath H_c t}|0\rangle. \tag{10}$$

Here H_c is the Hamiltonian of the core-excited state and E_0 is the ground-state energy. The stationary representation for T_m writes as follows:

$$T_m = -\imath\frac{\partial}{\partial\omega}\ln F_m = \frac{\imath}{F_m}\sum_n \frac{\langle m|n\rangle\langle n|0\rangle}{(\Omega - \varepsilon_n^c + \imath\Gamma)^2}. \tag{11}$$

The duration time is complex, $T_m = T_m' + \imath T_m''$, and consists of two different contributions [34]. The real part T_m' and the imaginary part T_m'' refer to the irreversible (decay) and reversible (dephasing) contributions, respectively, and depend differently on the detuning Ω and the core-hole lifetime Γ. T_m'' originates mainly from the detuning and can be named as the "dephasing time." This destructive interference supresses the long-time contribution to the scattering amplitude if the detuning is large.

Only decay transitions in the time domain $0 < t < |T_m|$ contribute significantly to F. The absolute value of the duration time is used exclusively for this reason,

$$\tau_m = [(T_m')^2 + (T_m'')^2]^{1/2}. \tag{12}$$

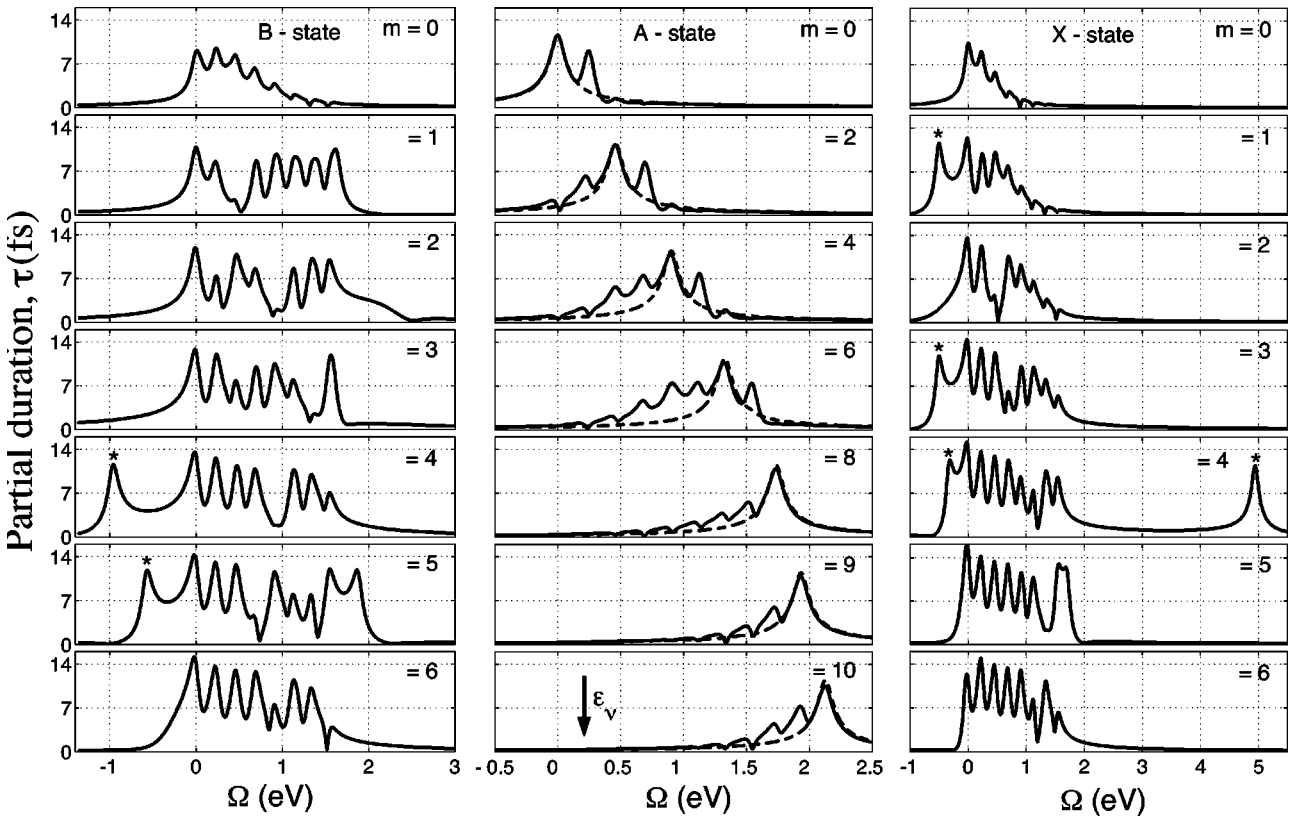

FIG. 6. Partial duration times, Eqs. (11) and (12), for different electronic-vibrational final states of N_2. The broken lines show the duration for the case when the potentials of the core-excited and the final states are the same ($1/\Gamma = 11.443$ fs, $\varepsilon_v \approx 92$ meV). The maxima related to some zeros of $\mathrm{Re}\, F_m$ are marked by stars.

The simulated duration times for different final states according to Eq. (12) (see Fig. 6), which are in agreement with the RPE profiles (see Figs. 1 and 2), demonstrate the shift of the region of slow scattering towards positive detunings (except for the maxima in Fig. 6 marked by an asterisk which will be discussed in Sec. V B 3). One can see a monotonic shift of the short wavelength flank of the $\tau_m(\Omega)$ to higher detunings with an increase of the final-state vibrational quantum number m. The reason for this was already mentioned above in Sec. V A 1: The scattering becomes fast when the vertical channel starts to dominate compared with the resonant one. This happens for $n \gtrsim 9$ and $n \gtrsim 6$ for A and B states, respectively. Apparently, the corresponding critical detuning depends strongly on the final electronic and vibrational states. In the RPE spectrum of the B state the vertical channel corresponds to the final vibrational levels $m = 0,1$, while the resonant channel corresponds to the group of levels with high binding energy. The strongest peaks at high binding energy correspond to the resonant channel for the A state. One can see that with increase of detuning, the different final vibrational states of the resonant channels disappear for different detunings: larger m corresponds to larger $\Omega \approx n\omega_c$. This correlation between m and n is very strong for the resonant channel of the A state [$m \approx n$ due to almost parallel potentials $U_c(R)$ and $U_f(R)$]. We can see the same trend for the duration time (see Fig. 6). To emphasize that the duration time is mainly related to the resonant channel, we calculated also τ_m for the same potential curves of the core-excited and A-final states (see broken lines in Fig. 6). In this case $m = n$ and the peak position of the duration follows Ω.

One can see from Fig. 6 that for some Ω the scattering becomes slower than the lifetime of the core-excited state, $\tau_m > 1/\Gamma = 11.443$ fs. This contradicts the physics and shows that our definition of the scattering duration, Eqs. (9) and (12), is not perfect. The main reason for this behavior is the above mentioned non-existence of a quantum-mechanical time operator. One encounters a similar problem in the definition of the tunneling time [36].

2. Mean duration of scattering

We need also the duration time which characterizes the whole RPE spectral profile. Clearly, the partial duration time τ_m, is not as important for the whole RPE spectral profile if the corresponding partial cross section $\sigma_m(E,\omega)$ is small. In other words, τ_m does not take into account that different final vibrational states m are represented in the RPE spectrum with different probabilities P_m. This motivates us to introduce the duration time for the whole RPE profile as the mean duration time τ,

$$\tau = \sum_m \tau_m P_m, \quad P_m = \frac{\sigma_m(\omega)}{\sigma(\omega)} \tag{13}$$

where

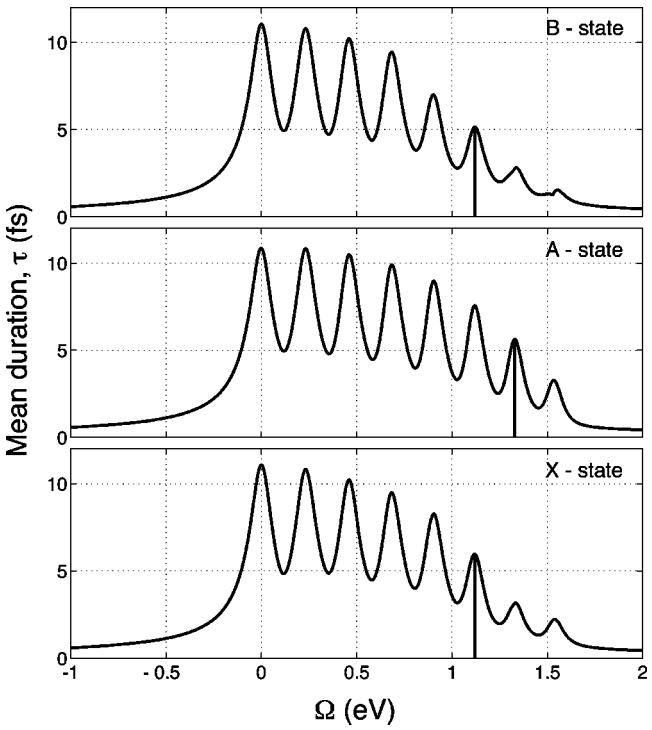

FIG. 7. The mean duration time, Eq. (13), for different final electronic states of N_2 vs detuning ($\Gamma = 0.0575$ eV). The positive detuning where the duration drops down in two times is shown by the vertical line.

$$\sigma_m(\omega) = \int \sigma_m(E,\omega)dE = |F_m|^2,$$

$$\sigma(\omega) = \sum_m \sigma_m(\omega) = \sum_m |F_m|^2 = \sum_n \frac{|\langle n|0\rangle|^2}{(\Omega - \varepsilon_n^c)^2 + \Gamma^2} \tag{14}$$

are the integral partial and total RPE cross sections. One can see that the total integral cross section copies the shape of the photoabsorption cross section in accordance with the optical theorem [37]. The simulation (see Fig. 7) shows that the mean duration is related more closely to the evolution of the gross features of the RPE profiles (see Figs. 1 and 2). In accordance with the measurements the larger τ are located in the region of positive detunings and the shift of the right-hand side flank of the $\tau = \tau(\Omega)$ distribution is larger for the A state.

3. The effect of zeros of $\mathrm{Re}\,F_m$ *on the scattering duration*

Figure 6 shows that the duration time has peaks (marked by stars) which are not related to the photoabsorption resonances. The position of these peaks coincide with the zeros Ω_c of $\mathrm{Re}\,F_m$:

$$\mathrm{Re}\,F_m(\Omega_c) = 0. \tag{15}$$

These values lie in both the region of strong photoabsorption and in the region of large $|\Omega|$. In the last case, $|\mathrm{Re}\,F| \gg \mathrm{Im}\,F$, because $\mathrm{Re}\,F \sim 1/\Omega$ and $\mathrm{Im}\,F \sim \Gamma/\Omega^2$. This means that the large root $|\Omega_c|$ of Eq. (15) corresponds to an almost complete quenching of the RPE cross section [28,33]. The formation of this interference quenching needs long time. Indeed, according to the uncertainty relation $\tau \sim 1/\Delta\Omega$ any sharp feature of the RPE cross section (resonance or minimum) takes a long time. Our simulations (see Fig. 6) show that τ_m increases in the vicinity of zeros of $\mathrm{Re}\,F$.

As it was observed recently [28,33] the zeros of the real part of the scattering amplitude can lead to an almost complete quenching of the the mth vibrational peak in the RPE spectrum. This effect takes place in the off-resonant region, $\Omega < 0$. Apparently, the complete quenching of $\mathrm{Re}\,F_m$ and of the related peak in the RPE spectrum is a pure interference effect [28,33]. One can see (see Figs. 2 and 4) that the RPE resonance, $m = 1$, vanishes for the X state when $\Omega = -0.5$ eV and it grows again for $\Omega > -0.5$ eV and $\Omega < -0.5$ eV. Fig. 8 illustrates that the origin of the quenching of this resonance is destructive interference. Indeed the direct term, $\sigma_{dir}(E,\omega)$, in the RPE cross section of the X

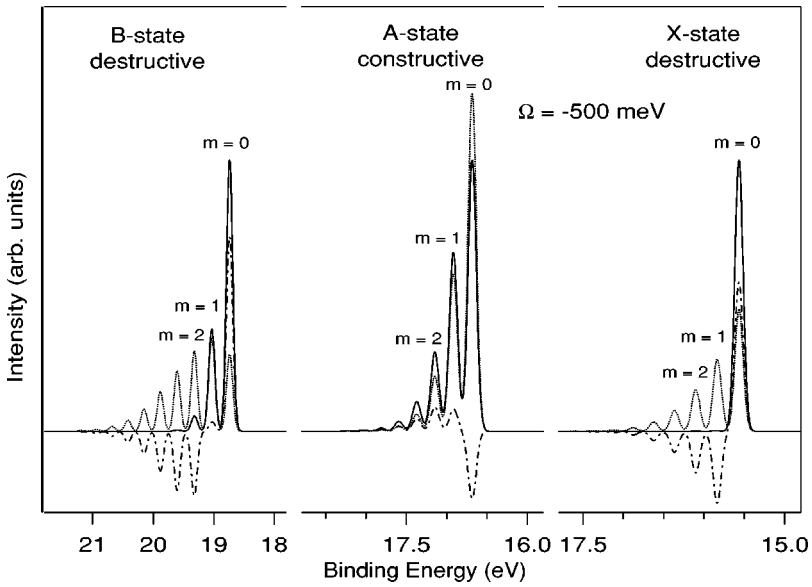

FIG. 8. Theoretical RPE profiles for $X\,^2\Sigma_g^+$, $A\,^2\Pi_u$, and $B\,^2\Sigma_u^+$ final states, ($\Omega = -500$ meV). The dashed, dashed-dotted, and solid lines represent the direct, $\sigma_{dir}(E,\omega)$, and interference, $\sigma_{int}(E,\omega)$, terms and the total, $\sigma(E,\omega) = \sigma_{dir}(E,\omega) + \sigma_{int}(E,\omega)$, RPE cross section, Eqs. (1) and (16), respectively. The observation of the collapse effect in the X and B final states can be explained in terms of ''destructive'' interference, and the observation of the buildup effect in the A state can be explained in terms of ''constructive'' interference.

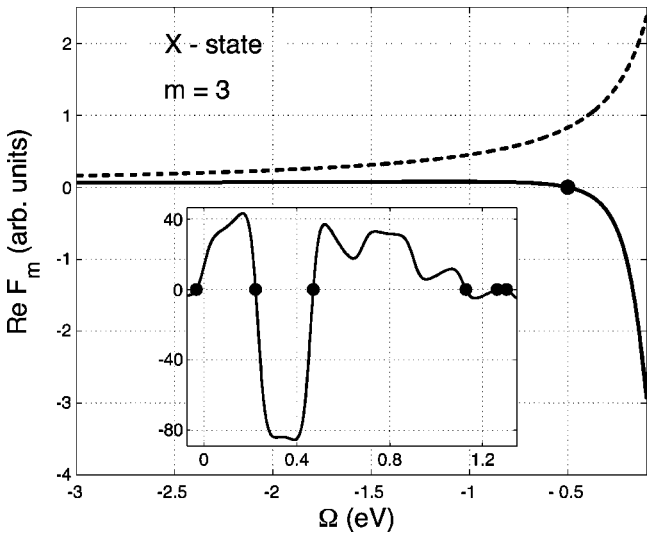

FIG. 9. The comparison of the strict scattering amplitude $\mathrm{Re}\,F_m$, Eq. (2), with the scattering amplitude $\mathrm{Re}\,F_m^S$ in the fast limit, Eq. (4), for $X\,^2\Sigma_g^+$ $(m=3)$ final state of N_2. The solid and broken lines represent $\mathrm{Re}\,F_m$ and $\mathrm{Re}\,F_m^S$, respectively. The inset shows other zeros of $\mathrm{Re}\,F_3$. The zeros of $\mathrm{Re}\,F_m$, Eq. (15), are shown by filled circles.

state is completely compensated by the negative interference contribution $\sigma_{int}(E,\omega)$. The direct and interference parts of $\sigma(E,\omega)=\sigma_{dir}(E,\omega)+\sigma_{int}(E,\omega)$ are defined by the first and the second terms on the right-hand side of the squared scattering amplitude [Eq. (2)],

$$|F_m|^2=\sum_n |F_{mn}|^2+\sum_{n\neq n_1} F_{mn}F_{mn_1}^* \tag{16}$$

in accordance with Eq. (1). It is worth to note that interference quenching of the resonance $m=1$ is absent for the *A* and *B* states. We see here also the quenching of higher vibrational peaks for the *B* and *X* states, but this is due to another effect, namely, the collapse effect [15,16] which has monotonic dependence on Ω. Near the zero Ω_c, Eq. (15), the scattering amplitude deviates significantly from the scattering amplitude of the fast RPE, Eq. (4) (see Fig. 9). In contrast, as we can see from Fig. 8, the buildup of a vibrational fine structure upon negative frequency detuning is due to constructive interference.

To conclude this section one can say that the scattering slows down near the zeros of $\mathrm{Re}\,F_m$ which can be located beyond the photoabsorption band (see Fig. 6).

C. The duration time versus spectral resolution and its compatibility with the Heisenberg uncertainty principle

The temptation exists to relate directly the duration time of the scattering process to the spectral resolution δE according to the Heisenberg uncertainty relation,

$$\delta E \sim \frac{1}{\tau}. \tag{17}$$

However, τ in the Heisenberg uncertainty relation refers to the time of interaction τ_{int} between light and matter, while the duration time [see Eqs. (11) and (12)] refers to the reversible interference discrimination of the large time contribution in the scattering process and has in this sense nothing to do with the time of interaction.

For example, when detuning the excitation energy from the resonance energy one changes the duration time according to Eq. (3). By exciting at photon energies far outside the resonance, all vibrational states of the resonance, which are intrinsically overlapping, are excited with a relative probability which is proportional to the relative strength of the specific vibrational state. This means in particular that even if one excites with a small photon energy bandpass, one will in fact not excite the resonant intermediate state with this resolution and hence will not only excite a specific vibrational level of the resonance, as the excitation bandwidth is solely determined by the properties of the intermediate state. The temporal resolution is, however, determined by Eq. (17). Hence, one excites for large detunings the resonant intermediate state for a very short time, but with a large energy spread [Eq. (17) is fulfilled]. However, due to the narrow photon energy bandpass one will still obtain high energy resolution in the resulting electron spectra, as one does not probe the final ionic state with high temporal resolution, but only the intermediate electronic state. In other words, large frequency detuning shortens the evolution of the molecule in the core-excited state with loss of the spectral resolution for the core excitation. However, one still keeps high resolution for the RPE resonance, $|0,0\rangle\rightarrow|f,m\rangle$, because the width of the Raman peak depends only on the spectral width of the incident light.

According to this discussion, we can conclude that, contrary to the pump-probe pulse technique the duration-time concept offers a unique possibility to make ''snapshots'' of physical-chemical processes without loss of the spectral resolution.

VI. SUMMARY

The concept of the duration time has provided an intriguing analysis tool for spectroscopical applications of the x-ray resonant Raman scattering process. In fact, owing to its simplicity it has formed the basis for predicting, and subsequently verifying, a set of new physical phenomena based on synchrotron radiation experiments, like, for example, ''restoration of symmetry selectivity'' [12,13], ''restoration of momentum selectivity'' [13,14], ''collapse of vibrational fine structure'' [15,16], ''control of dissociation'' [17–19], just to mention some of the main examples. The qualitative strength of the concept is thus indisputable, as well as its qualitative capacity to predict integrated band intensities, as can been seen, for example, from the original work on band formation of the resonant x-ray spectrum of CO_2 [12] and from more recent work on resonant photoemission spectra of HF [20]. Contrary to pump-probe techniques, the scattering duration sets the timing of the scattering process with a continuum wave light source. The duration of the scattering process then

acts effectively as a camera shutter with variable shutter speed.

The simplified picture claims that the scattering duration depends only on the potential of the core-excited state. This brings about the question on the applicability of the concept to quantitatively analyze ultrahigh resolution spectra where fine structure is sensitively dependent on the character of the final (vibronic) states. In this work we show that indeed the duration time of the scattering process in general depends on the final electronic and the final vibrational states. The physical reason behind this is that each final state ''selects'' certain coherent superpositions of the core-excited vibrational states.

The spectral features of the partial duration correlate with the main spectral features of the RPE. To characterize the gross features of the RPE profile it is, however, still useful to use the mean duration time. Both partial and mean duration times allow us to gain insight into the dynamics of the formation of the RPE spectra at ultrahigh resolution, as demonstrated here for the N_2 molecule. We have also shown that the transformation of the RPE spectral shape to the spectrum of the direct photoemission (fast RPE) can take place for detuning considerably larger than the effective width of the photoabsorption profile. The RPE spectrum converges to the fast limit only when the detuning exceeds the zeros of the real part of the scattering amplitude. The transition to the limit of the fast RPE depends also strongly on the competition between vertical and resonant scattering channels. Moreover, the transition to the fast scattering is very sensitive to the final-state potential. We see this clearly for different final states of N_2. The findings of the present work are general and cover also resonant radiative x-ray scattering.

ACKNOWLEDGMENTS

The authors acknowledge gratefully the support from the Swedish Research Council (VR), the Swedish Foundation for Strategic Research (SSF), the Swedish Foundation for International Cooperation in Research and Higher Education (STINT), the Knut and Alice Wallenberg Foundation, and the Göran Gustafsson Foundation. One of the authors (A.N.B.) wishes to acknowledge the National Council for Scientific and Technological Development (CNPq-Brazil) for financial support. R.F. would in particular like to thank VR and STINT for financial support of his stay at the Theoretical and Physical Chemistry Laboratory at Oxford University, United Kingdom. The collaboration of the staff of MAX-lab is gratefully acknowledged.

[1] T. Åberg and B. Crasemann, in *Resonant Anomalous X-Ray Scattering, Theory and Applications*, edited by G. Materlik, C. J. Sparks, and K. Fischer (North-Holland, Amsterdam, 1994), p. 431.
[2] E. Kukk, H. Aksela, A. Kivimäki, J. Jauhiainen, E. Nõmmiste, and S. Aksela, Phys. Rev. A **56**, 1481 (1997).
[3] Z.W. Gortel, R. Teshima, and D. Menzel, Phys. Rev. A **60**, 2159 (1999).
[4] F. Gel'mukhanov and H. Ågren, Phys. Rep. **312**, 87 (1999).
[5] F. de Groot, Chem. Rev. (Washington, D.C.) **101**, 1779 (2001).
[6] F.Kh. Gel'mukhanov, L.N. Mazalov, and A.V. Kondratenko, Chem. Phys. Lett. **46**, 133 (1977).
[7] Z.W. Gortel and D. Menzel, Phys. Rev. A **58**, 3699 (1998).
[8] M.N. Piancastelli, J. Electron Spectrosc. Relat. Phenom. **107**, 1 (2000).
[9] S.L. Sorensen and S. Svensson, J. Electron Spectrosc. Relat. Phenom. **114-116**, 1 (2001).
[10] J. Guo and J. Nordgren, J. Electron Spectrosc. Relat. Phenom. **110-111**, 105 (2000).
[11] H. Ågren, F. Gel'mukhanov, and P. Salek, J. Jpn. Soc. Synchrotron Rad. Res. **12**, 257 (1999).
[12] P. Skytt, P. Glans, J.-H. Guo, K. Gunnelin, J. Nordgren, F. Gel'mukhanov, A. Cesar, and H. Ågren, Phys. Rev. Lett. **77**, 5035 (1996).
[13] A. Cesar, F. Gel'mukhanov, Y. Luo, H. Ågren, P. Skytt, P. Glans, J.-H. Guo, K. Gunnelin, and J. Nordgren, J. Chem. Phys. **106**, 3439 (1997).
[14] T. Privalov, F. Gel'mukhanov, and H. Ågren, Phys. Rev. B **59**, 379 (1996).
[15] F. Gel'mukhanov, T. Privalov, and H. Ågren, Phys. Rev. A **56**, 256 (1997).
[16] S. Sundin, F. Gel'mukhanov, H. Ågren, S.J. Osborne, A. Kikas, O. Björneholm, A. Ausmees, and S. Svensson, Phys. Rev. Lett. **79**, 1451 (1997).
[17] F. Gel'mukhanov and H. Ågren, Phys. Rev. A **54**, 9243 (1999).
[18] P. Salek, F. Gel'mukhanov, and H. Ågren, Phys. Rev. A **59**, 1147 (1999).
[19] O. Björneholm, S. Sundin, S. Svensson, R.R.T. Marinho, A. Naves de Brito, F. Gel'mukhanov, and H. Ågren, Phys. Rev. Lett. **79**, 3150 (1997).
[20] A. Baev, P. Salek, F.Kh. Gel'mukhanov, H. Ågren, A. Naves de Brito, O. Björneholm, and S. Svensson, Chem. Phys. **00**, 0000 (2003).
[21] M. Bässler, A. Ausmees, M. Jurvansuu, R. Feifel, J.-O. Forsell, P. de Tarso Fonseca, A. Kivimäki, S. Sundin, S.L. Sorensen, R. Nyholm, O. Björneholm, S. Aksela, and S. Svensson, Nucl. Instrum. Methods Phys. Res. A **469**, 382 (2001).
[22] P. Baltzer, L. Karlsson, and B. Wanneberg, Phys. Rev. A **46**, 315 (1992).
[23] F. Gel'mukhanov and H. Ågren, Phys. Lett. A **193**, 375 (1994).
[24] S. Aksela, E. Kukk, H. Aksela, and S. Svensson, Phys. Rev. Lett. **74**, 2917 (1995).
[25] R. Feifel, A. Baev, F. Gel'mukhanov, H. Ågren, M. Bässler, G. Öhrwall, M.-N. Piancastelli, C. Miron, S. L. Sorensen, A. Naves de Brito, O. Björneholm, L. Karlsson, and S. Svensson, J. Electron Spectrosc. Relat. Phenom. **134**, 49 (2003).
[26] K.C. Prince, M. Vondracek, J. Karvonen, M. Coreno, R. Camilloni, L. Avaldi, and M. de Simone, J. Electron Spectrosc. Relat. Phenom. **101-103**, 141 (1999).
[27] K. P. Huber and G. Herzberg, *Molecular Spectra and Molecular Structure IV, Constants of Diatomic Molecules* (Van Nostrand Reinhold, New York, 1979).

[28] A. Baev, R. Feifel, F. Gel'mukhanov, H. Ågren, M.N. Piancastelli, M. Bässler, C. Miron, S.L. Sorensen, A. Naves de Brito, O. Björneholm, L. Karlsson, and S. Svensson, Phys. Rev. A **67**, 022713 (2003).

[29] R. Feifel, M. Andersson, G. Öhrwall, S.L. Sorensen, M.N. Piancastelli, M. Tchaplyquine, O. Björnehdm, L. Karlsson, and S. Svensson, Chem. Phys. Lett. **383**, 222 (2004).

[30] R. Feifel, L. Karlsson, M.-N. Piancastelli, R.F. Fink, M. Bässler, O. Björneholm, K. Wiesner, C. Miron, H. Wang, A. Giertz, S.L. Sorensen, A. Naves de Brito, and S. Svensson, Phys. Rev. A **65**, 052701 (2002).

[31] M.N. Piancastelli, R.F. Fink, R. Feifel, M. Bässler, S.L. Sorensen, C. Miron, H. Wang, I. Hjelte, O. Björneholm, A. Ausmees, S. Svensson, P. Salek, F.Kh. Gel'mukhanov and H. Ågren, J. Phys. B **33**, 1819 (2000).

[32] M.N. Piancastelli, A. Kivimäki, B. Kempgens, M. Neeb, K. Maier, U. Hergenhahn, A. Rüdel, and A. Bradshaw, J. Electron Spectrosc. Relat. Phenom. **98-99**, 111 (1999).

[33] R. Feifel, F. Gel'mukhanov, A. Baev, H. Ågren, M.N. Piancastelli, M. Bässler, C. Miron, S.L. Sorensen, A. Naves de Brito, O. Björneholm, L. Karlsson, and S. Svensson, Phys. Rev. Lett. **89**, 103002 (2002).

[34] F. Gel'mukhanov, P. Salek, T. Privalov, and H. Ågren, Phys. Rev. A **59**, 380 (1999).

[35] C. Miron, R. Feifel, O. Björneholm, S. Svensson, A. Naves de Brito, S.L. Sorensen, M.N. Piancastelli, M. Simon, and P. Morin, Chem. Phys. Lett. **359**, 48 (2002).

[36] V. Delgado, Phys. Rev. A **57**, 762 (1998).

[37] L. D. Landau and E. M. Lifshitz, *Quantum Mechanics-Non Relativistic Theory* (Addison-Wesley, Reading, MA, 1958).